



2025 Volume 30 Issue 4 Pages 604–625

https://doi.org/10.3846/mma.2025.22892

# A predation model considering a generalist predator and the Rosenzweig functional response

Viviana Rivera-Estay<sup>a</sup>, Alejandro Rojas-Palma<sup>b</sup> and Eduardo González-Olivares<sup>c</sup>

#### Article History:

- received December 10, 2024
- revised March 14, 2025
- accepted March 28, 2025

Abstract. This work deals with the dynamics of an ordinary differential equation system describing a Leslie-Gower predator-prey model with a generalist predator and a non-differentiable functional response proposed by M. L. Rosenzweig, given by  $h(x) = qx^{\alpha}$  with  $0 < \alpha < 1$ . Two aspects have a significant impact on the model: (1) the predator's carrying capacity depends on both the favorite prey population and an alternative food source, and (2) consumers have access to an alternative food source. Among the main results, a separatrix curve  $\Sigma$  arises dividing the phase plane into regions with different dynamic behaviors. Trajectories above the separatrix curve  $\Sigma$  reach the vertical axis in finite time, while those below  $\Sigma$  may converge to positive equilibrium points, limit cycles, or homoclinic connections. Furthermore, the system is non-Lipschitz, implying non-uniqueness of solutions at points of the vertical axis. Several bifurcations, including saddle-node, homoclinic, Hopf, generalized Hopf, and Bogdanov-Takens bifurcations, are identified through the use of computational techniques. The dynamics of the system are visualized by presenting a bifurcation diagram in a convenient parameter space.

Keywords: predator-prey model; Leslie-Gower model; separatrix; bifurcations; limit cycles; homoclinic

AMS Subject Classification: 92D25; 34C23; 58F14; 58F21.

#### 1 Introduction

The Gause type and the Leslie-Gower type models are the more usual patterns for the description of predator-prey interactions, by means of a nonlinear ordinary differential equation system. Leslie-Gower models are in contrast with Gause-type models in which the conversion of prey biomass into new predators follows a sort of mass-energy conservation law, being compartmentalized models [3]. Leslie-Gower formulations explicitly incorporate the dependence on the predator's population growth rate with respect to the quotient between

Copyright © 2025 The Author(s). Published by Vilnius Gediminas Technical University

This is an Open Access article distributed under the terms of the Creative Commons Attribution License (https://creativecommons.org/licenses/by/4.0/), which permits unrestricted use, distribution, and reproduction in any medium, provided the original author and source are credited.

<sup>&</sup>lt;sup>a</sup> Facultad de Ciencias, Universidad Arturo Prat, Arturo Prat Chacón 2120, Iquique, Chile

b Departamento de Matemática, Física y Estadística, Facultad de Ciencias Básicas, Universidad Católica del Maule, Talca, Chile

<sup>&</sup>lt;sup>c</sup>Pontificia Universidad Católica de Valparaíso, Valparaíso, Chile

<sup>☐</sup> Corresponding author. E-mail: ejgonzal@ucv.cl

the population sizes of predators and prey [20]. These models have been used in related fields, such as bioeconomics [8] and epidemiology.

An important issue in both types of models is the action of the predator that consumes the prey, called functional response or consumption rate [2,28]. In this work is depicted by a less-canonical function, which was proposed by the American ecologist Michael L. Rosenzweig in a seminal paper in 1971 [26]. This function is represented by  $h(x) = qx^{\alpha}$ , with  $0 < \alpha < 1$ , where x = x(t) is the prey population size [5,27] and is called power law [8] or Rosenzweig functional responses [14,25]. This function did not fit the three types of prey-dependent functional responses proposed by the biologist Crawford S. Holling in 1959 [16], because it is not bounded as the linear functional response l(x) = qx, being its main characteristic the non-differentiability when x = 0 [27]. The Rosenzweig functional response can be employed to describe a collective social behavior, known as prey herd behavior. This antipredator behavior (APB) occurs when individuals of one population gather in herds, either in search of food or for defensive purposes [1].

Additionally, this functional response has been proposed in the bioeconomic literature, where it is referred to as the compensatory power functional response [8]. The function is decreasing, with its components being the exponent  $\alpha$ , known as the *catchability exponent*, and the *variance in catchability q* [7]. It is a particular case of a more general function, known as the *Cobb-Douglas type production function*, given by  $h(x,y) = qx^{\alpha}y^{\beta}$ , with  $0 < \alpha, \beta < 1$ , [10,14]. This function has been widely used to describe the relationship between output and its inputs in an economic context. Here, x and y represent the capital and labor inputs, respectively (*i.e.*, the population involved in production), while q is a constant known as the *productivity factor*, and h denotes *total productivity* (the monetary value of all goods produced within a given period). The exponents  $\alpha$  and  $\beta$  refer to elasticities in an economic context.

In epidemiological models a power law has also been incorporated to represent a nonlinear incidence rate of the form  $h(I,S) = qI^{\alpha}S^{\beta}$ , with 0 < q,  $\alpha$ ,  $\beta$  [21], where S = S(t) and I = I(t) are the number of susceptible and infective individuals per unit area in the time  $t \geq 0$ , respectively; the parameter q is the transmission rate [21]. Particularly, when  $0 < \alpha$ ,  $\beta < 1$  is crucial to determine the existence of a region of persistence for a disease in the phase plane [21]. However, in many of the articles in which these functions are incorporated, the problem of the non differentiability at x = 0 is not studied, which has in general, a strong influence in the dynamics of the systems.

The fact that this Rosenzweig functional response is not differentiable at x=0 could have strong implications for the dynamics [12,30]. For instance, in Gause-type models with this functional response, the system is non-Lipschitzian, as two trajectories pass through each point on the vertical axis [5,27]. In the model proposed here, there is a separatrix curve determined by the stable manifold of a non-hyperbolic equilibrium. Trajectories with initial conditions above the separatrix curve will reach the vertical axis in finite time. This functional response is unsuitable for modeling interactions where the predator approaches satiety [23]. Furthermore, when incorporated into the basic Volterra model [28], it fails to satisfy the conditions of the Kolmogorov Theorem [22].

The system to be studied is based on the model [28], proposed by Philip H. Leslie in 1948 [20], who explicitly incorporates the dependence of this rate as the ratio between the population sizes of prey and predators. Leslie assumed that the equation for predators is a logistic-type growth function, in which the conventional environmental carrying capacity for predators  $K_y$  is proportional to the prey population size x = x(t), that is  $K_y = K(x) = nx$  [22, 28].

The model proposed by Leslie does not fit the Gause scheme and is not defined at x=0. For this reason, it has been strongly criticized for presenting anomalies in its predictions. Specifically, it forecasts that even at very low prey population densities, when the consumption rate per predator is almost zero, the predator population might still increase if the predator-to-prey ratio is very small [28]. Nonetheless, it is well-known that for the Leslie-Gower model [13] there exists a wide set of parameter values for which the unique positive equilibrium point is globally asymptotically stable [6, 11]. This property is proved by constructing a suitable Lyapunov function [17].

Leslie's model can be modified by adjusting the predator's carrying capacity to account for the presence of an alternative resource, assuming a generalist predator. Specifically, it was defined as  $K_y = K(x) = nx + c$ , where c is a positive constant. This implies that in the absence of prey (x) the predator can survive on this alternative food source [22,28].

This modified Leslie model was introduced in Díaz-Ávalos and González-Olivares (2017) [10], incorporating a Cobb-Douglas type production function as a functional response. That study established some fundamental properties of the model, such as the existence of an invariant region and the conditions for the existence and stability of equilibrium points, which were determined by defining different regions in the parameter space based on the values of  $\alpha$  and  $\beta$ . In particular, the case when  $\beta=1$  and  $\alpha\in(0,1)$ , which corresponds to the Rosenzweig functional response, was partially analyzed.

Building upon these findings, Rivera-Estay et al. (2020) [25] further explored this modified Leslie model with a Rosenzweig functional response, providing additional insights while still leaving some aspects open for further investigation. Their study addressed the existence and stability of equilibrium points, Hopf bifurcation conditions, and the existence of a separatrix. Furthermore, the case c=0 was examined, enabling a comparison with the case c>0. It was noted that simulations suggested the existence of solutions that approach the vertical axis in finite time (c>0). However, no formal proof of this phenomenon was provided. Lastly, simulations for the case c>0 were presented for specific parameter values, showing only cases where either a stable equilibrium or a stable limit cycle was observed.

In the present work, we extend the analysis of this model by examining the dynamics above the separatrix, providing a formal proof that the system is not Lipschitz. Additionally, we explore the various qualitative behaviors below the separatrix using bifurcation theory, which allows us to demonstrate the existence of new scenarios, such as a homoclinic connection and the existence of two concentric limit cycles. This approach provides valuable insights into the model's dynamics and unveils new results that highlight the system's complex behavior.

The main properties of the model were studied analytically. In particular, the nature of non-hyperbolic equilibrium points and an approximation of the separatrix curve were obtained. The dynamics of the model around the positive equilibrium points were partially analyzed analytically, as it was not possible to obtain an algebraic expression for them. However, we employed MATCONT (version 7.5), a MATLAB package for numerical continuation [9]. From this numerical analysis, we were able to construct a bifurcation diagram in a parameter space of interest, which allowed us to describe the different qualitative behaviors of the model.

The bifurcation diagram associated with the model reveals codimension-one bifurcations, such as saddle-node and Hopf bifurcations, as well as codimension-two bifurcations, including Bogdanov-Takens and Generalized Hopf bifurcations. In each region of the bifurcation diagram, the system exhibits different qualitative behaviors. For instance, in some regions, stable and unstable limit cycles coexist, while in others, these limit cycles merge and disappear through a saddle-node bifurcation. Additionally, we identified regions where a homoclinic connection forms as a result of the intersection of stable and unstable manifolds, and, in some cases, a limit cycle surrounded by a homoclinic connection emerges. These bifurcation phenomena reveal the complex dynamics of the model and provide insight into its topological transitions.

The rest of the paper is organized as follows: In Section 2, the modified Leslie-Gower model is presented; in Section 3, the main properties of model are proved; in Section 4, a bifurcation analysis of equilibrium points, periodic orbits and global connections (homoclinic phenomena). Finally, we summarize our main findings in Section 5.

## 2 Proposition of the model

For the construction of model describing the predator-prey interaction, the following assumptions are made:

- i) The model consists of one prey and one predator population.
- ii) The prey follows a logistic growth with a carrying capacity K and intrinsic growth rate r, which is reduced by the encounters with the predators.
- iii) The predator has a generalist feeding strategy. In fact, its carrying capacity depends on the prey population size x and other available food c. Therefore, even in the absence of the prey, the predator population follows a logistic growth with a carrying capacity nx + c and an intrinsic growth rate s.
- iv) The Rosenzweig functional response is chosen to represent the predators per capita feeding rates on the prey. It is represented by  $h(x) = qx^{\alpha}$ , with  $0 < \alpha < 1$ . The parameter  $\alpha$  determines the slope of the functional response near the origin and represents a kind of aggregation efficiency (see Figure 1).

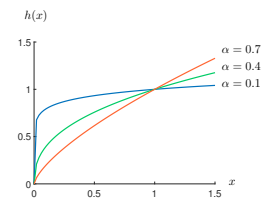


**Figure 1.** The graph of the functional response h(x) as it changes its steepness near x = 0 depending on the value of  $\alpha = 0.1$ ,  $\alpha = 0.4$  and  $\alpha = 0.7$ . Parameter q = 1 is fixed.

In view of the above assumptions the model takes the following form:

$$X_{\mu}(x,y):\begin{cases} \frac{dx}{dt} = r\left(1 - x/K\right)x - qx^{\alpha}y, \\ \frac{dy}{dt} = s\left(1 - \frac{y}{nx + c}\right)y, \end{cases}$$

$$(2.1)$$

where x = x(t) and y = y(t), denote the corresponding population sizes of the species as functions of time  $t \geq 0$  with x(0) > 0, and y(0) > 0. Moreover,  $\mu = (r, K, q, s, n, c, \alpha) \in \mathbb{R}^6_+ \times ]0, 1[$ , is the vector of parameters (see Table 1). Clearly, system (2.1) is defined in the first quadrant of  $\mathbb{R}^2$ , *i.e.*,

$$\varOmega=\big\{(x,y)\in\mathbb{R}^2/x\geq 0, y\geq 0\big\}.$$

The meanings of the positive parameters are given in the following table:

**Table 1.** Ecological parameters of the model.

Parameter	Ecological meaning
r	Intrinsic growth rate of the prey population.
K	Environmental carrying capacity of the prey
q	The consuming rate per capita of the predators.
s	Intrinsic growth rate of the predator population
n	The food quality and it indicates how the predators turn eaten prey into new predator births.
c	The quantity of alternative food for predators.
α	A shape parameter that determines the slope of the functional response near the origin and represents a kind of aggregation efficiency.

Since the functional response is given by  $h(x) = qx^{\alpha}$  with  $0 < \alpha < 1$ , system (2.1) is non-differentiable at x = 0. Consequently, an unconventional analysis is required to establish all the properties of the proposed model [25,27]. Additionally, the population sizes of both species cannot grow indefinitely, as the system's trajectories remain confined within a bounded region in the first quadrant, as will be demonstrated later.

Since (2.1) is differentiable in  $\Omega - (0, y)$ , the classical theory of ordinary differential equations ensures that there is uniqueness and smoothness of solutions for each initial condition in that domain [19].

To simplify the upcoming calculations, we transform system (2.1) into an equivalent form that is more convenient to handle. This transformation involves reparametrizing the vector field  $X_{\mu}$  through a change of variables and a time rescaling, as defined by:

$$\Phi: \mathbb{R}^2 \times \mathbb{R}_0^+ \to \mathbb{R}^2 \times \mathbb{R}_0^+, \quad \Phi\left(Ku, nKv, \tau(u+C)/r\right) \to (x, y, t).$$

The map  $\Phi$  is a diffeomorphism, due to det  $D\Phi(u, v, \tau) = \frac{nK^2(u+C)}{r} > 0$ . Let us consider new parameters defined by:  $\varphi : \mathbb{R}^6 \times ]0, 1[ \to \mathbb{R}^6 \times ]0, 1[$ 

$$\varphi(\mu) \to \left(r,K,n,\frac{qK^{\alpha}n}{r},\frac{c}{nK},\frac{s}{r},\alpha\right) = \left(r,K,n,Q,C,S,\alpha\right).$$

Since det  $D\varphi = \frac{K^{\alpha-1}}{r^2} > 0$ ,  $\varphi$  is invertible. As a result, the system (2.1) is transformed into a new vector field  $Y_{\eta} = \Phi_* X_{\mu} = (D\Phi)^{-1} \circ X_{\mu} \circ \Phi$ , which is given by:

$$Y_{\eta}(u,v):\begin{cases} \frac{du}{d\tau} = \left((1-u)u - Qu^{\alpha}v\right)(u+C),\\ \frac{dv}{d\tau} = S(u+C-v)v. \end{cases}$$
(2.2)

System (2.1) is  $C^{\infty}$ -equivalent to (2.2) in  $\Omega$  and it has the advantage of being defined with a reduced vector of parameters  $\eta = (Q, C, S, \alpha) \in \mathbb{R}^3 \times [0, 1[$ .

The system (2.2), or the vector field  $Y_{\eta}(u,v)$ , is defined in the first quadrant of  $\mathbb{R}^2$ , that is, in the set  $\overline{\Omega} = \{(u,v) \in \mathbb{R}^2 | u \geq 0, v \geq 0\}$ . The equilibrium points of system (2.2) are:  $p_0 = (0,0)$ ,  $p_u = (1,0)$ ,  $p_v = (0,C)$ , and the equilibria  $p_e = (u_e, v_e)$ , which represents coexistence, determined by the intersection of the isoclines. The abscissa of the positive equilibrium points, denoted by  $u_e$ , satisfies the transcendental equation:

$$q(u) = (1 - u)u - Qu^{\alpha}(u + C) = 0.$$
(2.3)

**Lemma 1.** Equation (2.3) has either one or two positive real roots.

*Proof.* See Appendix 6.1.  $\square$ 

Remark 1. According to Lemma 1, there can be at most two positive equilibria with an abscissa in the interval ]0,1[. The dynamics of the model studied here differ significantly from the model with c=0, where only a single positive equilibrium exists in the phase plane, with its abscissa within the interval ]0,1[.

#### 3 Results

#### 3.1 Main properties of the model

The following properties hold for system (2.2) or the vector field  $Y_{\eta}(u,v)$ :

**Lemma 2.** The set  $\overline{\Gamma} = \{(u,v) \in \overline{\Omega} : 0 \le u \le 1, v \ge 0\}$  is an invariant region.

*Proof.* See Appendix 6.2.  $\square$ 

Remark 2. Note that the set  $\overline{\Gamma}_C = \{(u,v) \in \overline{\Omega} : 0 \le u \le 1, v \le u + C\}$  is also an invariant region. The system (2.2) or the vector field  $Y_{\eta}(u,v)$  is of Kolmogorov type [12], as both axes are invariant sets.

**Lemma 3.** All solutions of system (2.2) which initiate in  $\mathbb{R}^2_+$  are uniformly bounded.

*Proof.* See Appendix 6.3.

**Lemma 4.** The equilibrium (1,0) is a hyperbolic saddle point for all parameter values.

*Proof.* See Appendix 6.4.  $\square$ 

**Lemma 5.** The equilibrium point (0,0) is a repeller point.

*Proof.* See Appendix 6.5.  $\square$ 

Remark 3. We define the set

$$\bar{\varLambda} = \Big\{ (u,v) \in \bar{\varGamma} : 0 \leq u \leq 1, \, 0 \leq v \leq v_{\varSigma}, \, \text{such that } \big( u,v_{\overline{\varSigma}} \big) \in \overline{\varSigma} \Big\},$$

such that the phase plane  $\bar{\Omega}$  is divided in the set  $\bar{\Lambda}$  and  $\overline{Z} = \bar{\Omega} - \bar{\Lambda}$ , where  $\overline{\Sigma}$  represents a separatrix curve, and  $\overline{Z}$  defines the region above this separatrix curve.

**Theorem 1.** The non-hyperbolic equilibrium point (0,C) has a hyperbolic and a parabolic sector [24] determined by the stable manifold  $W^s(0,C) = \overline{\Sigma}$ .

*Proof.* See Appendix 6.6.  $\square$ 

**Theorem 2.** All trajectories with initial conditions above the separatrix curve  $\overline{\Sigma}$  reach the v-axis in a finite time.

*Proof.* See Appendix 6.7.  $\square$ 

Remark 4. We have established Theorem 2 for the system (2.1), and this result also applies to the system (2.2), as both systems are topologically equivalent. The separatrix curve for system (2.1) is denoted by  $\Sigma$ . Note that the proof of Theorem 2 provides only a sufficient condition for prey extinction, not a necessary one, since the statement is proven for the region  $\bar{Z}$ , which lies above the separatrix curve  $\bar{\Sigma}$ .

Finding an analytical expression for  $\Sigma$  is a challenging task; however, we have derived a reliable approximation based on the approach outlined in [29] (see proof of Theorem 2 in the Appendix). This approximation is obtained

$$y(x) = \frac{x^{1-\alpha}\beta}{q(1-\alpha) - x^{1-\alpha}\beta}.$$

As a result of the above, the solutions along the vertical axis are non-unique. This presents a significant issue for this modeling approach, as the non-uniqueness of the solutions is counterintuitive, especially when compared to models used in Physics. In particular, the model does not meet Hadamard's conditions for well-posed problems [15].

Remark 5. As a result, the above theorem and the associated remark indicate that the system (2.1) is non-Lipschitzian along the vertical axis.

#### 3.2 Nature of positive equilibrium points

An explicit expression for the equilibria within the first quadrant cannot be determined, as  $0 < \alpha < 1$ . However, from the proof of Lemma 1 in Appendix 6.1, it is known that the system may have two, one, or no equilibrium points. To analyze the stability of these positive equilibrium points, we introduce a generic equilibrium point  $u_G$ . We define a new parameter G as follows:

$$Q: ]0,1[ \longrightarrow \mathbb{R}^+, \text{ such that } Q=Q(G):= rac{(1-G)G}{G^{lpha}(G+C)}.$$

The inverse function theorem ensures that one can locally define a unique  $G = G(Q) \in ]0,1[$  for every Q > 0. Let  $\xi := (C,S,G,\alpha) \in \mathbb{R} \times ]0,1[\times]0,1[$  be the new vector parameters. The field with parameters  $\xi$  is given by:

$$Y_{\xi}(u,v): \begin{cases} \frac{du}{d\tau} = \left((1-u)u - \frac{(1-G)G}{G^{\alpha}(G+C)}u^{\alpha}v\right)(u+C), \\ \frac{dv}{d\tau} = S(u+C-v)v. \end{cases}$$
(3.1)

Let us define the following functions  $f,g:\mathbb{R}\times\mathbb{R}\times ]0,1[\times ]0,1[\longrightarrow \mathbb{R}$  of parameters given by

$$f(\xi) = (1 - \alpha)G^2 + [2C + \alpha(1 - C)]G - C(1 - \alpha), \tag{3.2}$$

$$g(\xi) = 1 + \alpha(G - 1) - 2G - S.$$
 (3.3)

**Theorem 3.** The equilibrium point  $p_G = (G, G + C)$  satisfies the following:

- i) If  $\xi \in f^{-1}(\{0\})$ , the equilibrium  $p_G$  is not hyperbolic.
- ii) If  $\xi \in f^{-1}(]-\infty,0[)$ , the equilibrium  $p_G$  is a saddle.
- iii) If  $\xi \in f^{-1}(]0, +\infty[) \cap g^{-1}(]0, \infty+[)$ , the equilibrium  $p_G$  is a hyperbolic repeller.

iv) If  $\xi \in f^{-1}(]0, +\infty[) \cap g^{-1}(]-\infty, 0[)$ , the equilibrium  $p_G$  is a hyperbolic attractor.

v) If 
$$\xi \in f^{-1}(]0, +\infty[) \cap g^{-1}(\{0\})$$
, the equilibrium  $p_G$  is a weak focus.

*Proof.* See Appendix 6.8.  $\square$ 

Remark 6. Note that,  $f(\xi) = P_T(u)$ , then when  $P_T(u_T) = 0$  there is only one equilibrium point, which is not hyperbolic. On the other hand, from the proof of Lemma 1 in Appendix 6.1, it follows that  $P_T(u_T - \epsilon_2) < 0$  and  $P_T(u_T + \epsilon_1) > 0$ . Consequently, the equilibrium  $p_2 = (u_T - \epsilon_2, u_T - \epsilon_2 + C)$  is always a saddle point when it exists, and  $p_1 = (u_T + \epsilon_1, u_T + \epsilon_1 + C)$  can be either attractor or repeller when exists.

**Theorem 4.** The system (3.1) or vector field  $Y_{\xi}$  exhibits a saddle-node bifurcation at the equilibrium  $p_G$  when  $\xi \in f^{-1}(\{0\})$  and  $g^{-1}(]-\infty, 0[\cup ]0, +\infty[)$ .

*Proof.* See Appendix 6.9.  $\square$ 

Remark 7. The saddle-node bifurcation in Theorem 4 is a generically unfolded by parameter  $\alpha$  [18]. In particular, it follows that equation  $f(\xi) = 0$  implicitly defines the function

$$\alpha(C,G) = \frac{C - 2CG - G^2}{(G+C)(1-G)}$$
 and  $\frac{\partial f}{\partial \alpha} = 1 - G^2 \neq 0$ .

**Theorem 5.** The system (3.1) or vector field  $Y_{\xi}(u,v)$  exhibits a Hopf bifurcation at the equilibrium  $p_G$  when  $\xi \in (\theta^{-1}(]-\infty,0[)\cup\theta^{-1}(]0,\infty+[))\cap g^{-1}(0)$ , with  $\theta(\xi)=4Sf(\xi)+(C+G)\left(g(\xi)\right)^2$ .

*Proof.* See Appendix 6.10.  $\square$ 

Remark 8. The Hopf bifurcation in Theorem 5 is a generically unfolded by parameter  $\alpha$  [18]. In particular, it follows that equation  $g(\xi) = 0$  implicitly defines the function

$$\alpha(S,G) = \frac{S + 2G - 1}{G - 1} \quad \text{and} \quad \frac{\partial g}{\partial \alpha} = G - 1 \neq 0.$$

## 4 Numerical bifurcation analysis

The analysis of equilibria of system (2.2) in the interior of the first quadrant  $int\left(\overline{\varGamma}\right) = \left\{(u,v) \in \mathbb{R} : 0 < u < 1, v > 0\right\}$  is a major challenge, as it is generally not possible to obtain algebraic expressions for the coordinates of equilibria located in  $int(\overline{\varGamma})$ . Therefore, numerical tools are essential to continue the study. In this section, we present a bifurcation analysis performed using analytical tools from bifurcation theory to study codimension-1 bifurcations, and numerical continuation methods for codimension-2 bifurcations, utilizing the standard

continuation package MATCONT (version 7.5), which applies numerical continuation techniques such as predictor-corrector methods and Moore-Penrose pseudo-inverses to track equilibrium points and periodic orbits while detecting bifurcation points [9]. Additionally, MATCONT is grounded in analytical methods from bifurcation theory [19].

### 4.1 Bifurcation diagram in the $(\alpha, C)$ -plane

As a starting point, we consider S=0.4 and Q=1.2 fixed throughout this section and let  $\alpha$  and C to vary. The resulting bifurcation diagram in the  $(\alpha,C)$ -plane, is shown in Figure 2. This consists of a Hopf bifurcation curve labeled as  $H^+$  and  $H^-$  (blue curve), a saddle-node bifurcation curves labeled as LP (orange curve), a homoclinic bifurcation curve labeled as Hom (red curve) and saddle-node bifurcation of limit cycles labeled as LPC (green curve).

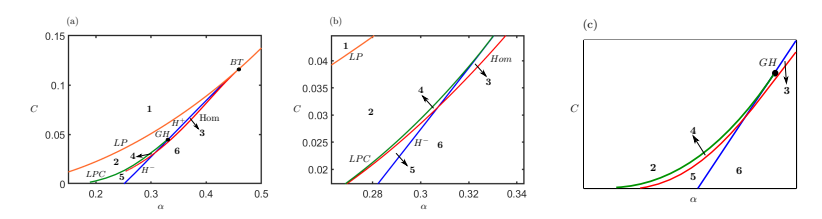


Figure 2. In (a) Bifurcation diagram of system (2.2) in the  $(\alpha, C)$ -plane. Parameter values S=0.4 and Q=1.2 are fixed. In (b) a zoom of bifurcation diagram. In panel (c) a qualitative sketch of the bifurcation diagram near the bifurcation point GH of system (2.2) in the  $(\alpha, C)$ -plane. Parameter values S=0.4 and Q=1.2 are fixed. Homoclinic curve (red curve) extends to C=0, progressing with the LPC curve (green curve) so that the region 4 narrows for smaller values of C, but it always has a non-empty interior.

There are two bifurcation points of codimension two that organize these curves. The point labeled as GH on the Hopf curve is a Generalized Hopf bifurcation point, from which the LPC curve emerges, This point divides the curve into two segments:  $H^+$  and  $H^-$ , corresponding to the subcritical and supercritical Hopf bifurcations, respectively. The point BT is a Bogdanov-Takens point, at which the curves LP, H and Hom meet. Figure 2(a) shows where the numerical convergence of the Hom curve ends (red curve), but this curve extends to C=0, progressing with the LPC curve so that the region narrows for smaller values of C, but it always has a non-empty interior as shown in Figure 2(c).

All the bifurcation events in Figure 2 are associated to positive equilibrium points and periodic orbits in  $int(\overline{\varGamma})$ . The curves in Figure 2 divide the shown part of the  $(\alpha, C)$ -plane into six open regions that we label as  $\mathbf{1}, \mathbf{2}, \mathbf{3}, \mathbf{4}, \mathbf{5}$  and  $\mathbf{6}$ , respectively. Now, we are going to explore how the bifurcation diagram in the parameter space  $(\alpha, C)$  changes as the parameter S changes. We construct three bifurcation diagrams for different values of parameter S and fixed Q = 1.2. The resulting bifurcation scenarios are shown in Figure  $\mathbf{3}(\mathbf{a})$ –(c).

In the three cases, the bifurcation diagrams in the  $(\alpha, C)$ -plane consists of a Hopf bifurcation curve labeled as H (blue curve), a saddle-node bifurcation

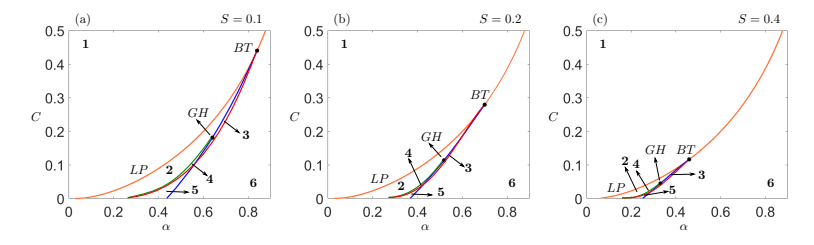


Figure 3. The bifurcation diagram in the  $(\alpha, C)$ -plane for different values of parameter S and fixed Q = 1.2. In panel (a) S = 0.1; In panel (b) S = 0.2; In panel (c) S = 0.4.

curves labeled as LP (orange curve), a homoclinic bifurcation curve labeled as Hom (red curve) and limit point of bifurcation cycles labeled as LPC (green curve). There are two bifurcation points of codimension two that organize these curves. The point BT is a Bogdanov-Takens point, at which the curves H, LP and Hom meet. The second point is a Generalized Hopf point, labelled as GH, at which the curves H and LPC meet.

Let us note that as the parameter S increases, the curve LP remains in the same position, while the point BT moves towards the origin along the curve LP (orange curve), in a manner similar to the movement of point GH along the curve H (blue curve). Hence, the curves H, LPC and Hom became shorter, resulting in a reduction of regions  $\mathbf{2}$ ,  $\mathbf{3}$ ,  $\mathbf{4}$  and  $\mathbf{5}$ , while region  $\mathbf{6}$  increases (see Figure  $3(\mathbf{a})$ –(c)).

#### 4.2 Phase portraits

In order to explore how the dynamics of system (2.2) change as we move from one region to another in the parameter space  $(\alpha, C)$ , the Figure 4 shows partial renditions of six possible phase portraits in  $\overline{\Gamma}$ . In the region 1 there are no equlibria points. As the point  $(\alpha, C)$  crosses the curve LP from region 1 into region 2, two equilibria—labelled as  $p_1$  (unstable focus) and  $p_2$  (saddle point) appear in the interior of  $\overline{\Gamma}$  via a saddle-node bifurcation. If  $(\alpha, Q)$  moves from region 2 into region 3 by crossing the curve  $H^+$  (blue curve), one unstable limit cycle appears around the equilibria  $p_1$  via Hopf bifurcation (see Figure 4(a)). A family of unstable periodic orbits exists in the interior of  $\overline{\Gamma}$  for (Q, S) in region 3, if (Q,S) reaches the Hom curve (red curve), the family of cycles converges to a homoclinic orbit. More precisely, the homoclinic orbit is a connection between the stable and unstable manifolds of  $p_2$  (see Figure 4(b)). Finally, in region 6, the homoclinic connection is broken.

If  $(\alpha, C)$  moves from region **3** into region **4** by crossing the curve  $H^-$  (see Figure 2(b)), a stable limit cycle appears, *i.e.*, in region **4** there are two limit cycles around the unstable focus  $p_1$  (see Figure 4(c)). The stable limit cycle is inside the unstable limit cycle. If  $(\alpha, Q)$  moves from region **4** into region **2** by crossing the LPC curve, both limit cycles collapse and disappear due to a saddle-node bifurcation of limit cycles. In region **4** if  $(\alpha, Q)$  reaches curve Hom the (red curve) the family of unstable limit cycles converges to a homoclinic orbit (see Figure 4(d)). Meanwhile, in region **5** homoclinic connection is broken,

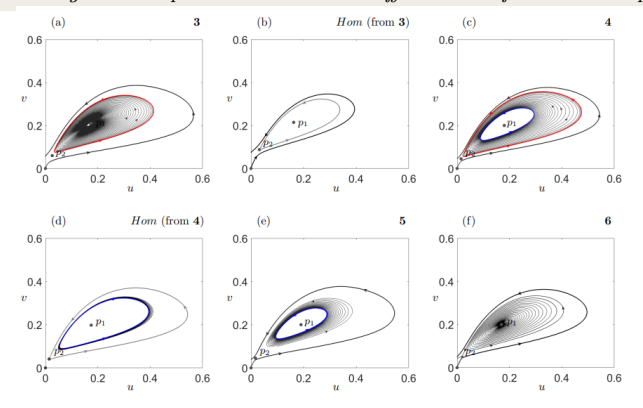


Figure 4. Phase portraits of system (2.2) corresponding to the bifurcation diagram in Figure 3. Parameter values are  $(\alpha, C) = (0.318, 0.037) \in \text{region 3}$  in panel (a);  $(\alpha, C) = (0.2899, 0.024515) \in Hom$  in panel (b);  $(\alpha, C) = (0.306, 0.0312) \in \text{region 4}$  in panel (c);  $(\alpha, C) = (0.354475, 0.054747) \in Hom$  in panel (d);  $(\alpha, C) = (0.3, 0.028) \in \text{region 5}$  in panel (e);  $(\alpha, C) = (0.304, 0.0324) \in \text{region 5}$  in panel (f). Parameter values S = 0.4 and Q = 1.2 are fixed.

but the stable limit cycle remains (see Figure 4(e)). Finally, as the point  $(\alpha, C)$  crosses the  $H^-$  curve from region **5** into region **6**, the stable limit cycles disappear (see Figure 4(f)). In region **6** there are two equilibria—labelled as  $p_1$  (stable focus) and  $p_2$  (saddle point) which disappear in region **1** via a saddle-node bifurcation.

#### 4.3 Bifurcation diagram and its associated phase portraits

Figure 5 provides a qualitative illustration of the bifurcation diagram and its corresponding phase portraits. The central panel shows the bifurcation curves in the  $(\alpha, C)$  parameter space, while the surrounding panels depict the phase portraits for different regions of this space. This diagram may help in better understanding the transition of dynamics as we move through the  $(\alpha, C)$  parameter space.

In region 1 there are not equilibriums points. In region 2 there are two equilibrium point  $p_1$  (unstable focus) and  $p_2$  (saddle point) which emerge by saddle node bifurcation. In region 3 an unstable limit cycle emerges through a Hopf bifurcation, which surrounds  $p_1$  (stable focus). On the Hom curve (from region 3), a homoclinic connection is formed, where the unstable and stable manifolds of  $p_2$  connect. In region 6 the homoclinic connection is broken, but both  $p_1$  (stable focus) and  $p_2$  (saddle point) remain. In region 5 a stable limit cycle emerges through a Hopf bifurcation, which surrounds  $p_1$  (unstable focus). On the Hom curve (from region 4), a homoclinic connection forms, where the unstable and stable manifolds of  $p_2$  connect, and the stable limit cycle persists. In region 4, the homoclinic connection is broken, and an unstable limit cycle emerges, resulting in two limit cycles surrounding  $p_1$  (unstable focus). Due to a saddle-node bifurcation of limit cycles, these limit cycles collapse into a single cycle along the LPC curve, eventually disappearing in region 2.

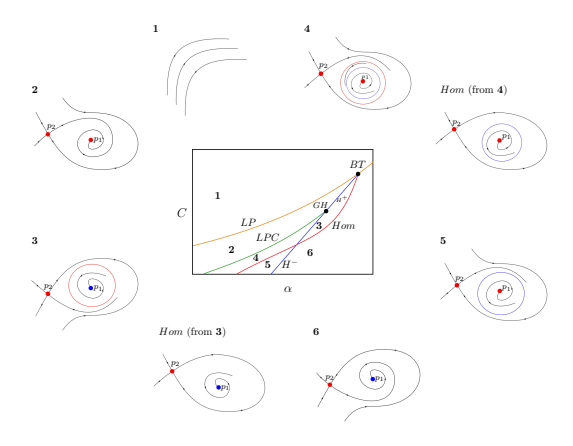


Figure 5. Qualitative illustration of the bifurcation diagram and phase portraits. The central panel shows bifurcation curves in the  $(\alpha, C)$  space, including saddle-node (LP), saddle-node of limit cycle (LPC), homoclinic (Hom), and Hopf (blue) bifurcations. The Hopf curve splits into supercritical  $(H^-)$  and subcritical  $(H^+)$  branches, separated by the generalized Hopf bifurcation point (GH). Surrounding panels show phase portraits for different parameter regions, with  $p_1$  and  $p_2$  as positive equilibrium points. Parameter values S = 0.4 and Q = 1.2 are fixed.

#### 5 Conclusions

In this work, we present a more comprehensive analysis of the dynamic behaviors of the modified Leslie model, addressing aspects not explored in previous studies. Building on the results of Díaz-Ávalos & González-Olivares (2017) [10] and Rivera-Estay et al. (2020) [25], we provide a deeper understanding of the model's complexity. Specifically, we analyze the dynamics of a modified Leslie-Gower predation model [13,17], which exhibits novel behaviors involving generalist predators. A key feature is the non-differentiable functional response of the predator, described by  $h(x) = qx^{\alpha}$ , with  $0 < \alpha < 1$ , and the assumption that the predator's carrying capacity depends on prey population size, expressed as  $K_y = K(x) = nx + c$ , with c > 0.

To simplify the calculations, the system was reparameterized and the time was rescaled, obtaining a topologically equivalent system. It was proven that the new system obtained (2.2) is differentiable at the origin, which is a continuous extension of the original one. Besides, it was proved that the solutions of the system are bounded, implying the model is well-posed [3].

We show the existence of a separatrix curve  $\Sigma$ , determined by the stable manifold of the hyperbolic equilibrium (0,C), which divides the behaviors of the trajectories on the phase plane. The trajectories within region Z, located above the separatrix curve  $\Sigma$ , eventually intersect the vertical axis [29] in finite time, similar to what occurs in the Volterra model with the Rosenzweig functional response [27]. Consequently, the modified Leslie-Gower model is non-Lipschitzian along the vertical axis, as two solutions of the system pass through each point on that axis.

An ecologically interesting result is the nature of the non-hyperbolic equilibrium, whose stable manifold  $W^s\left(0,C\right)$  divides the phase plane into two complementary sectors. This point acts as an attractor for trajectories along the separatrix curve determined by  $W^s\left(0,C\right)$ . Thus, a high predator population size leads to the extinction of their preferred prey. This is a desirable outcome when the prey constitutes a pest. However, if the prey are a species of interest, such as commercially exploited fish, precautions should be taken to avoid their extinction.

It was established that the system can have up to five singularities; the origin  $(p_0)$ , two equilibria over the axis  $(p_u \text{ and } p_v)$ , and positive equilibrium points  $(p_1 \text{ and } p_2)$ . The equilibriums  $p_u$  is always a hyperbolic saddle. The origin and  $p_v = (0, C)$  are non-hyperbolic and its stability can be proven using sophisticated mathematical techniques, such as changes in convenient variables. It was not possible to find an algebraic expression for the equilibrium  $p_1$  and  $p_2$ . However, through geometric and analytical tools, it was possible to prove that  $p_2$  is always a hyperbolic saddle, and that  $p_1$  can be an attractor or a repeller, depending on specific parameter conditions.

It provides the explicit conditions under which the equilibrium  $p_1$  an undergo saddle-node and Hopf bifurcations. Additionally, a numerical bifurcation analysis reveals the existence of various types of bifurcations. In fact, using MATCONT, a MATLAB package for numerical continuation [9], we identified two codimension-two bifurcations: Bogdanov-Takens and Generalized Hopf. These bifurcation were identified in the parameter space  $(\alpha, C)$  as a bifurcation points labeled BT and GH. From these points, bifurcation curves emerge, dividing the parameter space into open regions. All these points and curves form the bifurcation diagram in the parameter space  $(\alpha, C)$ , where S and Q are fixed. Additionally, as the parameter S increases, the bifurcation diagram shifts towards the origin, causing most of the regions in the first quadrant of the  $(\alpha, C)$ -plane to decrease in size.

In each region of the bifurcation diagram, the system exhibits distinct qualitative behaviors, characterized by different phase portraits within the first quadrant. For instance, for specific parameter values, the system can simultaneously exhibit two limit cycles: one stable and one unstable. As we move to another region, these limit cycles collapse and disappear through a saddle-node bifurcation. Furthermore, in another region, the stable and unstable manifolds  $p_2$  can connect, forming a homoclinic orbit. This homoclinic connection arises from a family of limit cycles whose periods converge to infinity. Lastly, there are regions where the system can exhibit a limit cycle surrounded by a homoclinic connection. Therefore, the bifurcation diagram provides insight into the topological transitions within the model's dynamics [19].

These numerical results deepen our understanding of the system's dynamics, essential for describing ecological scenarios. The numerical bifurcation analysis identifies specific conditions for persistence through a stable equilibrium point or a stable limit cycle. Furthermore, when two limit cycles exist (one stable and one unstable) not only can we confirm that persistence occurs through the stable limit cycle, but we can also determine the thresholds for the initial populations necessary for persistence, based on the basin of attraction of the

stable limit cycle. Specifically, this basin is bounded by the unstable limit cycle. A similar situation arises in regions where a stable limit cycle is surrounded by a homoclinic connection, and in this case, the basin is bounded by the homoclinic connection.

These properties make a clear difference with the dynamics of the model proposed by P. H. Leslie in 1948 [20]. It has a unique positive equilibrium point which is globally asymptotically stable. it has also a remarkable difference with the model Leslie-Gower model considering the Rosenzweig functional response, but with c=0 [13], which is lipschitzian on the vertical axis. Future work could identify heteroclinic connections through analytic study and bifurcation analysis in other parameter spaces. Another study will explore the effect of an Allee effect on prey while maintaining Rosenzweig functional responses.

#### Acknowledgements

This work was partially supported by the UCM-IN-23202 grant. V.R.E. also thanks Pablo Aguirre for his valuable comments.

#### References

- [1] V. Ajraldi, M. Pittavino and E. Venturino. Modeling herd behavior in population systems. *Nonlinear Analysis: Real World Applications*, **12**(4):2319–2338, 2011. https://doi.org/10.1016/j.nonrwa.2011.02.002.
- [2] A.D. Bazykin. Nonlinear dynamics of interacting populations, volume 11 of World Scientific Series on Nonlinear Science, Series A. World Scientific, Singapore; River Edge, NJ, 1998. https://doi.org/10.1142/2284.
- [3] A.A. Berryman, A.P. Gutierrez and R. Arditi. Credible, parsimonious and useful predator-prey models: a reply to Abrams, Gleeson, and Sarnelle. *Ecology*, 76(6):1980–1985, 1995. https://doi.org/10.2307/1940728.
- [4] G. Birkhoff and R. Gian-Carlo. Ordinary differential equations. John Wiley & Sons, New York, NY, 1989.
- [5] J.L. Bravo, M. Fernández, M. Gámez, B. Granados and A. Tineo. Existence of a polycycle in non-Lipschitz Gause-type predator-prey models. *Journal of mathematical analysis and applications*, 373(2):512–520, 2011. https://doi.org/10.1016/j.jmaa.2010.08.001.
- [6] C. Chicone. Ordinary differential equations with applications, volume 34 of Texts in Applied Mathematics. Springer-Verlag, New York, 2 edition, 2006.
- [7] Colin W Clark. The worldwide crisis in fisheries: economic models and human behavior. Cambridge University Press, 2006.
- [8] C.W. Clark. Mathematical Bioeconomics. In P. van den Driessche(Ed.), Mathematical Problems in Biology, volume 2, pp. 29–45, Berlin, Heidelberg, 1974. Springer, Springer Berlin Heidelberg. https://doi.org/10.1007/978-3-642-45455-4\_3.
- [9] A. Dhooge, W. Govaerts and Yu.A. Kuznetsov. MATCONT: a MAT-LAB package for numerical bifurcation analysis of ODEs. ACM Transactions on Mathematical Software (TOMS), 29(2):141–164, 2003. https://doi.org/10.1145/779359.779362.

- [10] J. Díaz-Avalos and E. González-Olivares. Dynamics of a predator-prey model with a non-differentiable functional response. In J. Vigo-Aguiar(Ed.), Proceedings of the 17th International Conference on Computational and Mathematical Methods in Science and Engineering (CMMSE 2017), volume 3, pp. 765-776, Costa Ballena, Rota, Cádiz, Spain, 2017. Arizona State University.
- [11] F. Dumortier, J. Llibre and J.C. Artés. Qualitative theory of planar differential systems, volume 2 of Universitext. Springer-Verlag, Berlin, Heidelberg, 1 edition, 2006. https://doi.org/10.1007/978-3-540-32902-2.
- [12] H.I. Freedman. Deterministic mathematical models in population ecology, volume 57 of Pure and Applied Mathematics. Marcel Dekker Incorporated, New York, 1980.
- [13] E. González-Olivares and V. Rivera-Estay and A. Rojas-Palma and K. Vilches-Ponce. A Leslie-Gower type predator-prey model considering herd behavior. Ricerche di Matematica, 73(4):1683-1706, 2024. https://doi.org/10.1007/s11587-022-00694-5.
- [14] E. González-Olivares, E. Sáez, E. Stange and I. Szantó. Topological description of a non-differentiable bioeconomics model. The Rocky Mountain Journal of Mathematics, 35(4):1133-1155, 2005. https://doi.org/10.1216/rmjm/1181069680.
- [15] J. Hadamard. Lectures on Cauchy's problem in linear partial differential equations, volume 15 of Yale Studies in Mathematics. Yale university press, New Haven, CT, 1923.
- [16] C.S. Holling. The components of predation as revealed by a study of small-mammal predation of the European pine sawfly. *The Canadian Entomologist*, 91(5):293–320, 1959. https://doi.org/10.4039/Ent91293-5.
- [17] A. Korobeinikov. A Lyapunov function for Leslie-Gower predator-prey models. Applied Mathematics Letters,  $\bf 14(6):697-699$ , 2001. https://doi.org/10.1016/S0893-9659(01)80029-X.
- [18] Y. Kuang and H.I. Freedman. Uniqueness of limit cycles in Gause-type models of predator-prey systems. Mathematical Biosciences, 88(1):67–84, 1988. https://doi.org/10.1016/0025-5564(88)90049-1.
- [19] Y.A. Kuznetsov. Elements of applied bifurcation theory, volume 112 of Applied Mathematical Sciences. Springer-Verlag, New York, 2 edition, 1998. https://doi.org/10.1007/978-1-4612-0745-9.
- [20] P.H. Leslie. Some further notes on the use of matrices in population mathematics. Biometrika, 35(3-4):213–245, 1948. https://doi.org/10.1093/biomet/35.3-4.213.
- [21] W.-M. Liu, S.A. Levin and Y. Iwasa. Influence of nonlinear incidence rates upon the behavior of SIRS epidemiological models. *Journal of Mathematical Biology*, 23(2):187–204, 1986. https://doi.org/10.1007/BF00276956.
- [22] R.M. May. Stability and Complexity in Model Ecosystems. Princeton Landmarks in Biology. Princeton University Press, Princeton, NJ, 2 edition, 2001. https://doi.org/10.1515/9780691206912. Reprint of the 1973 work with a new introduction
- [23] M.R. Myerscough, M.J. Darwen and W.L. Hogarth. Stability, persistence and structural stability in a classical predator-prey model. *Ecological Modelling*, 89(1-3):31–42, 1996. https://doi.org/10.1016/0304-3800(95)00117-4.

- [24] L. Perko. Differential equations and dynamical systems, volume 7 of Texts in Applied Mathematics. Springer-Verlag, New York, 3 edition, 2001. https://doi.org/10.1007/978-1-4613-0003-8.
- [25] V. Rivera-Estay, E. González-Olivares, A. Rojas-Palma and K. Vilches-Ponce. Dynamics of a class of Leslie-Gower predation models with a non-differentiable functional response. In H. Dutta and J.F. Peters(Eds.), Applied Mathematical Analysis: Theory, Methods, and Applications, volume 177 of Studies in Systems, Decision and Control, pp. 433–457. Springer, Cham, 2019. https://doi.org/10.1007/978-3-319-99918-0\_14.
- [26] M.L. Rosenzweig. Paradox of enrichment: destabilization of exploitation ecosystems in ecological time. Science, 171(3969):385–387, 1971. https://doi.org/10.1126/science.171.3969.385.
- [27] E. Sáez and I. Szántó. A polycycle and limit cycles in a non-differentiable predator-prey model. Proceedings – Mathematical Sciences, 117(2):219–231, 2007. https://doi.org/10.1007/s12044-007-0018-9.
- [28] P. Turchin. Complex Population Dynamics: A Theoretical/Empirical Synthesis, volume 35 of Monographs in Population Biology. Princeton University Press, Princeton, 2003.
- [29] E. Venturino and S. Petrovskii. Spatiotemporal behavior of a prey-predator system with a group defense for prey. *Ecological Complexity*, 14:37–47, 2013. https://doi.org/10.1016/j.ecocom.2013.01.004.
- [30] K. Vilches, E. González-Olivares and A. Rojas-Palma. Prey herd behavior modeled by a generic non-differentiable functional response. *Mathematical Modelling of Natural Phenomena*, **13**(3):26, 2018. https://doi.org/10.1051/mmnp/2018038.

## 6 Appendix

## 6.1 Proof of Lemma 1 (Number of positive real roots)

Let  $v=\frac{1}{Qu^{\alpha}}(1-u)u$  and v=u+C the isoclines curve. Considering the tangency of the isoclines, it has  $\frac{d}{du}\left(u+C\right)=1$ , and  $\frac{d}{du}\left(\frac{1}{Qu^{\alpha}}\left(1-u\right)u\right)=-\frac{1}{Qu^{\alpha}}\left(2u+\alpha-u\alpha-1\right)$ . Then, equaling both derivatives we have  $-2u-\alpha+u\alpha+1=Qu^{\alpha}$ . Besides,  $Qu^{\alpha}=\frac{(1-u)u}{v}=\frac{(1-u)u}{u+C}$ . Therefore,  $\frac{(1-u)u}{u+C}=-2u-\alpha+u\alpha+1\Leftrightarrow (1-u)u-(-2u-\alpha+u\alpha+1)\left(u+C\right)=0$ , and the abscissa  $u_T$  of the tangency point satisfy the polynomial equation  $P_T\left(u\right)=(1-\alpha)u^2+\left[\alpha+C(2-\alpha)\right]u-C\left(1-\alpha\right)=0$ . Applying Descartes' rule of signs  $P_T(u)$ , the polynomial has a unique positive root, since  $0<\alpha<1$ , which is given by:

 $u_T = \frac{1}{2(1-\alpha)} \left( -\left(\alpha + C\left(2-\alpha\right)\right) + \sqrt{\Delta_T} \right)$ , with  $\Delta_T = \left[\alpha + C(2-\alpha)\right]^2 + 4C(1-\alpha)^2 > 0$ , which is positive for all  $0 < \alpha < 1$  and C > 0. Figure 6 shows that the isoclines can intersect at two, one, or no points. Both isoclines intersect at one point at  $u_T$  ( $P_T(u_T) = 0$ ), and when they intersect at two points, there exist positive real values  $\epsilon_1$  and  $\epsilon_2$  such that  $u_1 = u_T + \epsilon_1$  and  $u_2 = u_T - \epsilon_2$ . Additionally, it gets

$$P_T(u_T - \epsilon_2) = \epsilon_2 \left[ u_T(\alpha - 1) + (\epsilon_2 - u_T) + \alpha (u_T - \epsilon_2 - 1) + C(\alpha - 2) \right] < 0, P_T(u_T + \epsilon_1) = (1 - \alpha) \left( 2u_T \epsilon_1 + \epsilon_1^2 \right) + \epsilon_1 \left[ \alpha + C(2 - \alpha) \right] > 0.$$

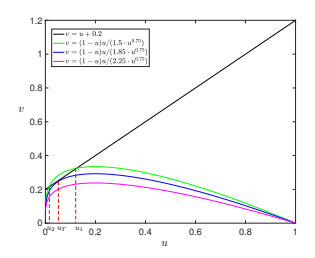


**Figure 6.** Relative positions of the isoclines, when v = u + 0.2, and  $v = (1 - u)u/(Qu^{0.75})$ , for Q = 1.5 (green curve), 1.85 (blue curve) and 2.25 (purple curve).

#### 6.2 Proof of Lemma 2 (Existence of a positively invariant region)

We consider u = 1, thus we obtain

$$Y_{\eta}(1,v): \begin{cases} \frac{du}{d\tau} = -Qv, \\ \frac{dv}{d\tau} = S(1+C-v)v. \end{cases}$$

Hence, orbits with initial conditions outside of the set will enter to  $\overline{\Gamma}$ ; the trajectories inside of this set will not leave it.

#### 6.3 Proof of Lemma 3 (Boundedness of solutions)

From the first equation of system (2.2) it becomes  $\frac{du}{d\tau} \leq (1-u)(u+C)u^2$ ,  $\forall v \in \mathbb{R}^+$ . We have that  $u(\tau) \to 1$ , when  $\tau \to \infty$  and u < 1. Furthermore,  $u(\tau) \to 1$ , when  $\tau \to \infty$  and u > 1. Defining  $L = \max \{u(0), 1\}$ , it has  $u(\tau) \leq L$ ,  $\forall \tau, v \geq 0$ . We consider  $W(\tau) = u + \frac{1}{S}v$ ; then,

$$\frac{dW(\tau)}{d\tau} = \frac{du}{d\tau} + \frac{1}{S}\frac{dv}{d\tau} = \left( (1-u)u - Qu^{\alpha}v \right) (u+C) + (u+C-v)v.$$

Then,

$$\begin{split} &\frac{dW(\tau)}{d\tau} + \sigma W(\tau) = Cu - Cu^2 + Cv + uv + u^2 - u^3 - v^2 - CQu^{\alpha}v - Qu^{1+\alpha}v \\ &+ \sigma \left(u + v/S\right) \leq Cu + Cv + uv + u^2 - v^2 + \sigma u + \frac{\sigma}{S}v = -v^2 + v\left(C + u + \sigma/S\right) \\ &+ Cu + u^2 + \sigma u = -\left[v - \left(\frac{CS + uS + \sigma}{2S}\right)\right]^2 + \left(\frac{CS + uS + \sigma}{2S}\right)^2 + Cu + u^2 + \sigma u \\ &\leq \left(\frac{CS + uS + \sigma}{2S}\right)^2 + Cu + u^2 + \sigma u \leq \left(\frac{CS + S + \sigma}{2S}\right)^2 + C + 1 + \sigma = R. \end{split}$$

Then,  $0 \leq \frac{dW(\tau)}{d\tau} + W(\tau) \leq R$ , which is a first-order linear inequality. By the Comparison Theorem for differential inequality [4], we obtain  $W(\tau)e^{\tau} \leq Re^{\tau} + C$ . When  $\tau = 0$ ,  $W(0) \leq R + C$ . There is  $n \in N$  such that  $C \leq n (W(0) - R)$ , then  $W(\tau)e^{\tau} \leq e^{\tau}R + n (W(0) - R)$ ,  $W(\tau) \leq R + e^{-\tau}n (W(0) - R)$ . Clearly, when  $\tau \to \infty$  then  $W(\tau) \leq R$ .

#### 6.4 Proof of Lemma 4 (Nature of singularity (1,0))

The Jacobian matrix of system (2.2) is

$$DY_{\eta}(u,v) = \begin{pmatrix} -(C+u)\left(2u + \frac{Q\alpha u^{\alpha}v}{u} - 1\right) + ((1-u)u - Qu^{\alpha}v) & -Qu^{\alpha}(C+u) \\ Sv & S(u+C-2v) \end{pmatrix}.$$

Then, evaluated in (1,0) is:

$$DY_{\eta}(1,0) = \begin{pmatrix} -1-C & -(1+C)Q \\ 0 & (1+C)S \end{pmatrix},$$

whose eigenvalues are  $\lambda_1 = -1 - C < 0$ ,  $\lambda_2 = (1 + C)S > 0$ . The result follows because  $\det DY_n(1,0) = -(S + 2CS + C^2S) < 0$ .

#### 6.5 Proof of Lemma 5 (Nature of singularity (0,0))

From the above, it can be observed that one component of the Jacobian matrix  $DY_{\eta}$  is undefined at u=0. A change of variables is introduced to enable the evaluation of the equilibrium at (0,0). Let  $u=X^{1/1-\alpha}$  and v=Y and apply a time rescaling  $T=\left(X^{1/1-\alpha}+C\right)(1-\alpha)\tau$ . After performing algebraic calculations, we obtain the system:

$$\hat{Y}_{\eta}\left(X,Y\right):\begin{cases} \frac{dX}{dT} = X - X^{\frac{\alpha-2}{\alpha-1}} - QY, \\ \frac{dY}{dT} = SY\left(-X^{1/1-\alpha} - C + Y\right)\left(X^{1/1-\alpha} + C\right)^{-1} (1-\alpha)^{-1}. \end{cases}$$
(6.1)

The Jacobian matrix of the system  $\hat{Y}_{\eta}(X,Y)$  is:

$$D\hat{Y}_{\eta}(X,Y) = \begin{pmatrix} a_{11} & a_{12} \\ a_{21} & a_{22} \end{pmatrix}, \text{ with}$$

$$a_{11} = \left[\alpha - 1 - (\alpha - 2)X^{\frac{1}{1-\alpha}}\right](\alpha - 1)^{-1}, \quad a_{12} = -Q,$$

$$a_{21} = X^{\frac{\alpha}{1-\alpha}}Y^{2}(\alpha - 1)\left(C + X^{\frac{1}{1-\alpha}}\right)^{2},$$

$$a_{22} = \left(-C - X^{\frac{1}{1-\alpha}} + 2Y\right)\left(X^{1/1-\alpha} + C\right)^{-1}(\alpha - 1)^{-1}.$$

Evaluating the matrix  $D\hat{Y}_{\eta}(X,Y)$  in the point (0,0) we obtain:

$$D\hat{Y}_{\eta}(0,0) = \begin{pmatrix} 1 & -Q \\ 0 & S(1-\alpha)^{-1} \end{pmatrix}.$$

Therefore, equilibrium point (0,0) is a repeller.

### 6.6 Proof of Theorem 1 (Nature of singularity (0, C))

The Jacobian matrix  $DY_{\eta}$  is not defined in u=0. A change of variables is introduced to allow the evaluation of the equilibrium (0,C). Let  $u=X^{\frac{2}{1-\alpha}}$  and v=Y, and apply a time rescaling  $T=\frac{2X}{1-\alpha}\tau$ . After performing the algebraic calculations, we obtain the system:

$$\overline{Y}_{\overline{\eta}}(X,Y) : \begin{cases}
\frac{dX}{dT} &= \left[ \left( 1 - X^{\frac{2}{1-\alpha}} \right) X^2 - QY \right] \left( X^{\frac{2}{1-\alpha}} + C \right), \\
\frac{dY}{dT} &= BXY \left( X^{\frac{2}{1-\alpha}} + C - Y \right),
\end{cases} (6.2)$$

where  $\overline{\eta} = (Q, C, B, \alpha)$  with  $B = \frac{2S}{1-\alpha}$ . Note that  $\overline{Y}_{\overline{\eta}}(0, Y) = -CQY\frac{\partial}{\partial X}$ . Then, the orbits of the vector field in Equation (6.2) are orthogonally crossing the X = 0 axis (Y > 0). Let  $\overline{\gamma}$  be an orbit of the vector field in Equation (6.2), and there exists an orbit  $\gamma$  of the system in Equation (2.2), which is tangent to the vector field  $Y_{\eta}$  at the point  $(0, v_0)$ , with  $v_0 > C$ . Clearly, the u = 0 axis is an invariant manifold, and  $Y_{\eta}(0, v_0) = -Sv_0(v_0 - C)\frac{\partial}{\partial v}$ . Thus, at the point  $(0, v_0)$ , there exist at least two orbits. Therefore, the system in Equation (2.2) is non-Lipschitzian. The vector field in Equation (6.2) is a differentiable extension of the vector field in Equation (2.2), and (0, C) is an equilibrium point for both systems. However,

$$D\overline{Y}_{\overline{\eta}}(0,C) = \begin{pmatrix} 0 & -CQ \\ 0 & 0 \end{pmatrix}.$$

It considers the horizontal blowing-up to desingularize (0, C) [11]. Let X = u and Y = uv. After performing some calculations, we obtain the system:

$$J_{\overline{\eta}}\left(u,v\right):\begin{cases} \frac{du}{dT}=u\left[u(1-u^{\frac{2}{1-\alpha}})-Qv\right]\left(u^{\frac{2}{1-\alpha}}+C\right),\\ \frac{dv}{dT}=v\left[Bu\left(u^{\frac{2}{1-\alpha}}+C-uv\right)-\left(u\left(1-u^{\frac{2}{1-\alpha}}\right)-Qv\right)\left(u^{\frac{2}{1-\alpha}}+C\right)\right],\end{cases}$$

where, 
$$DJ_{\overline{\eta}}(0,C) = \begin{pmatrix} 0 & 0 \\ 0 & 0 \end{pmatrix}$$
.

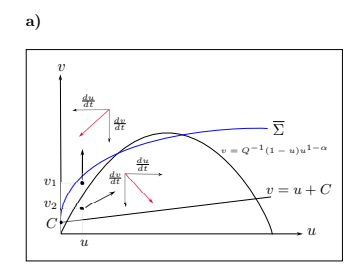
Now, considering the vertical blowing-up to desingularize (0, C) [11]. Let u = XY and v = Y. After some calculations, we obtain the system:

$$\begin{cases} \frac{dX}{dT} = & XY \left[ 2\left(X\left(1 - \left(XY\right)^{\frac{2}{1-\alpha}}\right) - Q\right) \left(\left(XY\right)^{\frac{2}{1-\alpha}} + C\right) \\ & -BX\left(\left(XY\right)^{\frac{2}{1-\alpha}} + C - XY^2\right) \right] \\ \frac{dY}{dT} = & Y^2 \left[ BX\left(\left(XY\right)^{\frac{2}{1-\alpha}} + C - XY^2\right) - \left(X\left(1 - \left(XY\right)^{\frac{2}{1-\alpha}}\right) - Q\right) \left(\left(XY\right)^{\frac{2}{1-\alpha}} + C\right) \right], \end{cases}$$

with 
$$D\tilde{J}_{\overline{\eta}}(0,C) = \begin{pmatrix} -2C^3Q & 0 \\ 0 & 2C^2Q \end{pmatrix}$$
.

Since the vector field  $\hat{Y}\eta$  in Equation (6.1) is  $C^1(R+^2, R_+^2)$ , by the Existence and Uniqueness Theorem, a unique trajectory  $\gamma$  passes through (0, C), corresponding to the separatrix  $\overline{\Sigma}$  in the topologically equivalent system  $Y_{\eta}$ . Considering the isocline:

$$v = Q^{-1} (1 - u) u^{1 - \alpha}. (6.3)$$



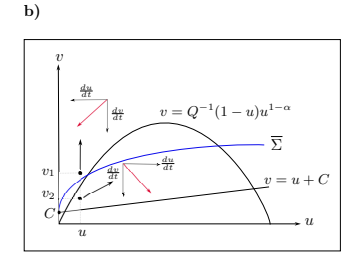


**Figure 7.** Figure illustrative of proof. Black curves represent isoclines and blue curve presents separatrix, which divides the plane (u, v) into a hyperbolic and a parabolic sector. In panel a) the separatrix is obove  $(u, v_1)$  and in panel b) the separatrix is below  $(u, v_2)$ .

For fixed u such that u < v - C, there exist  $v_1$  and  $v_2$  such that  $(u, v_1)$  lies below the separatrix  $\overline{\Sigma}$  and above the isocline, while  $(u, v_2)$  lies below both the isocline and the separatrix. If this relation holds consistently, we have  $\frac{dv}{d\tau}(u, v_1) < 0$  and  $\frac{du}{d\tau}(u, v_1) < 0$ ; furthermore,  $\frac{dv}{d\tau}(u, v_2) < 0$  and  $\frac{du}{d\tau}(u, v_2) > 0$  (see Figure 7(a)). Suppose the separatrix lies below the isocline for a certain value in the first quadrant. Then, for the points above the isocline in Equation (6.3), we have  $\frac{du}{d\tau} < 0$ . Therefore, for trajectories with an initial condition in  $(u, v_1)$  as t increases for t > 0, these trajectories would cross the separatrix  $\overline{\Sigma}$ , which contradicts the uniqueness of solutions within the interior of the first quadrant. Then, for all sufficiently small 0 < u, there exist  $v_1, v_2$  such that  $(u, v_1)$  and  $(u, v_2)$  are above and below the separatrix  $\overline{\Sigma}$ , respectively (see Figure 7(b)). Hence, there is an hyperbolic sector.

#### 6.7 Proof of Theorem 2 (Extinction of prey in finite time)

It will be shown for the system (2.1). Let  $x_0 = x(0)$  and  $y_0 = y(0)$  be initial conditions for the system (2.1) and let R be the part of the phase plane defined as  $R = \{(x, y)/x > 0, y > \tilde{y}(x)\}$ , where  $\tilde{y}(x) = x^{1-\alpha}\beta/(q(1-\alpha)-x^{1-\alpha}\beta)$ . Considering the equations of the system (2.1) we have:

Considering the equations of the system (2.1) we have: 
$$\frac{dy}{dt} = s \left(1 - \frac{y}{nx+c}\right) y \ge -\frac{y^2}{nx+c} \ge -\frac{y^2}{nx+c} - \frac{y}{nx+c} \ge -\frac{y^2}{c} - \frac{y}{c}.$$

Then, by virtue of the Comparison Theorem for differential inequality [4],  $\hat{y}$  is the solution of the equation  $\frac{d\hat{y}}{dt} = \frac{1}{c}(-y^2 - y)$ , corresponding to the same initial condition  $\hat{y}(0) = y(0) = y_0$ ; then  $y(t) \geq \hat{y}(t) = \frac{y_0}{e^{\delta t}(y_0+1)-y_0}$ , for any t > 0 and  $\delta = 1/n$ . Besides,

$$\frac{dx}{dt} = r\left(1 - \frac{x}{K}\right)x - qx^{\alpha}y \le rx - qx^{\alpha}y \le rx - qx^{\alpha}\hat{y} \le rx - qx^{\alpha}\frac{y_0}{e^{\delta t}(y_0 + 1)}.$$

Therefore, again by the Comparison Theorem for differential inequality [4], if  $\hat{x}$  is the solution of the equation

$$\frac{d\hat{x}}{dt} = r\hat{x} - q\hat{x}\frac{y_0}{e^{\delta t}(y_0 + 1)},\tag{6.4}$$

corresponding to the same initial condition  $\hat{x}(0) = x(0) = x_0$ ; then  $x(t) \leq \hat{x}(t)$ , for any t > 0. In order to solve (6.4), we introduce a new variable W(t) defined as  $\hat{x}(t) = W(t)e^{rt}$ . It has that  $W(0) = \hat{x}(0) = x(0)$ . From definition of W and (6.4), we obtain the following equation for the derivative of W:

$$\frac{dW}{dt} = -\frac{W^{\alpha}qy_0e^{-\beta t}}{y_0+1}$$
, where  $\beta = r(1-\alpha) + \delta$ .

As W(0) > 0 and the second term in the right-hand side of the above derivative is a monotonically increasing function of t. It means that  $W(t^*) = 0$  for a certain  $t^*$ , if and only if,  $W(0)^{1-\alpha} = \left[qy_0(1-\alpha)\right]/\left[\beta(y_0+1)\right]$ . Taking into account the relation between W and  $\hat{x}$ , it is obvious that  $W(t^*) = 0$  is equivalent to  $\hat{x}(t^*) = 0$ . Since  $W(0) = x_0$ , from above equation we obtain that  $\hat{x}(t^*) = 0$  for any  $x_0$  and  $y_0$  satisfying the following condition:  $y_0 > x_0^{1-\alpha}\beta/\left[q(1-\alpha)-x_0^{1-\alpha}\beta\right]$ . Recalling that  $\hat{x}$  is an upper bound for x(t); if  $\hat{x}(t^*) = 0$  then  $x(t^*) \leq 0$ ; this means that x(t) becomes zero for some  $\hat{t} \leq t^*$ . Since x(t) cannot become negative (because the axis x=0 is a part of the x-isocline in the phase plane of system (2.1), x(t)=0 for any  $t \geq \hat{t}$ . Therefore, the last inequality provides a sufficient condition for the prey species extinction. That completes the proof.

#### 6.8 Proof of Theorem 3 (Nature of positive equilibrium point)

The Jacobian matrix  $DY_{\xi}(p_G)$  is

$$DY_{\eta}(G, G+C) = \begin{pmatrix} (G+C)(1-2G-\alpha(1-G)) & -(1-G)G\\ S(G+C) & -S(G+C) \end{pmatrix}.$$

It is easy to check that det  $DY_{\eta}(G, G+C) = S(C+G)f(\xi)$  and  $TrDY_{\eta}(G, G+C) = (C+G)g(\xi)$ , where f and g are defined in (3.2) and (3.3), respectively. It follows from the Hartman-Grobman's theorem that the equilibrium  $p_G$  is a repeller (resp. attractor) for (3.1) if  $\xi \in f^{-1}(]0, +\infty[) \cap g^{-1}(]0, \infty+[)$  (resp.  $\xi \in f^{-1}(]0, +\infty[) \cap g^{-1}(]-\infty, 0[)$ ).

#### 6.9 Proof of Theorem 4 (Existence of a saddle node bifurcation)

Let  $p_G = (G,G+C)$  a generic equilibrium point and the conditions for a saddle node bifurcation are: i) det  $DY_{\eta}(G,G+C) = 0$ ; ii)  $TrDY_{\eta}(G,G+C) \neq 0$ ; iii) (Transversality condition)  $\frac{\partial \left(\det DY_{\eta}(G,G+C)\right)}{\partial C} \neq 0$ .

#### 6.10 Proof of Theorem 5 (Existence of a Hopf bifurcation)

According to the previous proof, for parameter values  $\xi$  in a neigbourhood of the set  $f^{-1}\left(]-\infty,0[\right)\cap g^{-1}(0)\subset\mathbb{R}\times]0,1[\times]0,1[$ , the eigenvalues of the system (3.1) have the form  $\lambda_{1,2}=\beta(\xi)\pm i\omega(\xi)$ , where  $\beta(\xi)=\frac{1}{2}g(\xi)$  and  $\omega(\xi)=\frac{1}{2}\sqrt{\left(C+G\right)\left[4Sf(\xi)+\left(C+G\right)\left(g(\xi)\right)^2\right]}$ . In particular, if  $g(\xi)=0$ , then  $\beta(\xi)=0$ . Moreover,  $\frac{\partial g}{\partial S}=-1$  and, hence,  $\frac{\partial \beta}{\partial S}\neq 0$ . Therefore, the real part  $\beta(\xi)$  changes sign every time the parameter vector  $\xi$  crosses the level set  $g^{-1}(0)\subset\mathbb{R}\times]0,1[\times]0,1[$ . Moreover,  $\omega(\xi)=0$  if and only if  $\theta(\xi)=0$ , where  $\theta(\xi)=4Sf(\xi)+(C+G)\left(g(\xi)\right)^2$ . Hence, if  $\xi\in\left(\theta^{-1}(]-\infty,0[)\cup\theta^{-1}(]0,\infty+[)\right)\cap g^{-1}(0)$ , the system  $Y_\xi$  exhibits a Hopf bifurcation at the equilibrium  $p_G$ .